SIMSAND Implementation on the Geotechnical Particle Finite Element Method G-PFEM

David León-Vanegas[1], Lluís Monforte [2] and Marcos Arroyo [1,2]
1. Universitat Politècnica de Catalunya (UPC-BarcelonaTECH), Barcelona, Spain
2. Centre Internacional de Mètodes Numèrics en Enginyeria (CIMNE), Barcelona, Spain
08034 Barcelona (SPAIN)
david.eduardo.leon@upc.edu

Abstract: This paper presents a large-strain implementation of the SIMSAND on the Geotechnical Particle Finite Element Method (G-PFEM). SIMSAND is a simple, critical-state-based constitutive model, which captures the density and pressure dependent behaviour of sands. The formulation adopts a large-strain hyperelastic–plastic framework that employs the Kirchhoff stress tensor and the Hencky strain tensor instead of their small-strain counterparts. Local integration is performed using a multiplicative decomposition of the deformation gradient and an explicit integration scheme with sub-stepping error control adapted to large strain. Global convergence is enhanced through the IMPLEX scheme and a non-local regularization to alleviate mesh dependence during strain-softening dominated simulations. The implementation is validated through drained and undrained triaxial simulations using both single-Gauss-point element tests and boundary-value problems. Comparation with experimental data for Fontainebleau sand NE34 shows that the model successfully reproduces contractive and dilative behaviour, as well as peak and post-peak softening. The resulting framework provides a robust tool for modelling large deformation geomechanical problems, with planned applications to cone penetration test and pile installation in sands.

Keywords: SIMSAND, state parameter, sands, G-PFEM, large deformation

1 Introduction

In granular materials such as sand, particle-scale mechanisms such as grain sliding, rolling, interlocking, and grain crushing control the macroscopic behaviour, leading to non-linear stress-strain responses with hardening or softening and volumetric changes involving contraction and dilation (Rowe, 1962). These particle-scale mechanisms depend on density and confining stress (Been & Jefferies, 1985); therefore, to accurately capture sand behaviour, constitutive models based on critical state soil mechanics (CSSM) (Schofield & Wroth, 1968) are required.

Various CSSM constitutive models for sand have been developed, such as NorSand (Jefferies, 1993), CASM (Yin et al., 2020), Severn-Trend (Gajo & Wood, 1999), SANISAND (Dafalias & Manzari, 2004; Taiebat & Dafalias, 2008), and SIMSAND (Yin et al., 2020). Among these, the latter stands out for its efficient and straightforward formulation. SIMSAND is a model with a shear yield mechanism, in which the peak strength and dilatancy are functions of the state parameter, enabling it to capture the strength and compressibility response of sand at different densities and stress states using the same set of parameters.

This paper presents a large strain formulation of the SIMSAND model and its implementation in the software Geotechnical Particle Finite Element Method G-PFEM (Carbonell et al., 2022). The implementation is validated by simulating a triaxial test in Fontainebleau sand NE34 using a single Gauss point solution (elementary test) and boundary value solutions.

2 SIMSAND

The SIMSAND model developed by Yin et al. (2020) is a stress-ratio controlled, critical state-based model featuring nonlinear plastic hardening. It can be viewed as an extension of the Mohr-Coulomb model incorporating isotropic hardening.

The yield surface of SIMSAND is an open cone in three-dimensional space, so loading at an isotropic compression direction results in only elastic deformation. The model could be enhanced by incorporating volumetric or cap mechanics, as illustrated by Hu et al. (2011) or Leon-Vanegas et al. (2025).

2.1 *Elasticity*

In the G-PFEM, SIMSAND is formulated for finite strains, using the Kirchhoff stress tensor $\tau_{ij} = J\sigma_{ij}$ as a measure of stress, where σ_{ij} is the Cauchy stress tensor and $J = \det(F_{ij})$ is the Jacobian or determinant of the deformation gradient F_{ij}. As a measure of strain, the Hencky strain tensor $\epsilon_{ij} = \frac{1}{2}\ln(F_{ik}\,F_{kj})$ is utilized. Furthermore, the Kirchhoff stress tensor is computed directly by derivation of a free energy function W, i.e., $\tau_{ij} = \partial W(\epsilon_{ij}^e)/\partial\epsilon_{ij}^e$, in particular, the free energy function defined by Houlsby et al. (2005) is used:

$$
\begin{aligned}
W &= \frac{p_a}{k(2-n)}\left[k(1-n)\nu_0\right]^{\left(\frac{2-n}{1-n}\right)} \\
\mathrm{v}_0^2 &= \left[\epsilon_{ii}^e + \frac{1}{k(1-n)}\right]\left[\epsilon_{jj}^e + \frac{1}{k(1-n)}\right] + \frac{2g\; e_{ij}^e e_{ij}^e}{k(1-n)}
\end{aligned}
\tag{1}
$$

where $\epsilon_{ij}^e = \frac{1}{2}\ln(F_{ik}^e\,F_{kj}^e)$ is the Hencky elastic strain tensor, $e_{ij}^e = \epsilon_{ij}^e - \frac{1}{3}\epsilon_{kk}^e\delta_{ij}$ is the deviatoric part of the Hencky elastic strain tensor, p_a is a reference pressure, k, g and n are material parameters that represent the bulk stiffness factor, the shear stiffness factor and the pressure exponent, respectively.

The stiffness elastic matrix is derived from the Kirchhoff stress tensor or from the second derivative of the free energy function $D_{ijkl}^e = \partial^2 W/\partial\epsilon_{ij}^e\partial\epsilon_{kl}^e$. The full expression of this stiffness matrix is presented in Houlsby et al. (2005).

In a triaxial formulation the free energy function can be written in terms of volumetric strain $\epsilon_v = \epsilon_{ii}^e$ and deviatoric strain $\epsilon_d = \sqrt{\frac{2}{3}e_{ij}^e e_{ij}^e}$ invariants, i.e. $W(\epsilon_v, \epsilon_d)$. Then, the increment of Kirchhoff mean effective stress, $\pi = \frac{1}{3}\tau_{ii}$, and Kirchhoff deviatoric invariant $q = \sqrt{3/2 s_{ij}s_{ij}}$, with $s_{ij} = \tau_{ij} - \pi\delta_{ij}$ being the deviatoric part of the Kirchhoff stress tensor, is computed by the incremental stiffness matrix presented in Equation (2).

$$\begin{bmatrix} \dot{\pi} \\ \dot{q} \end{bmatrix} = \begin{bmatrix} \frac{\partial^2 W}{\partial \epsilon_v} & \frac{\partial^2 W}{\partial \epsilon_v \partial \epsilon_d} \\ \frac{\partial^2 W}{\partial \epsilon_v \partial \epsilon_d} & \frac{\partial^2 W}{\partial \epsilon_d} \end{bmatrix} \begin{bmatrix} \dot{\epsilon_v} \\ \dot{\epsilon_d} \end{bmatrix} = \begin{bmatrix} K & J \\ J & G \end{bmatrix} \begin{bmatrix} \dot{\epsilon_v} \\ \dot{\epsilon_d} \end{bmatrix} \tag{2}$$

where K and G are the tangent bulk and shear moduli, and J is a coupling modulus between volumetric and deviatoric behaviour. This coupling modulus arises from the hyper-elastic formulation and produces stress-induced anisotropy because the elastic matrix has non-zero diagonal terms (Houlsby et al., 2005). Those moduli are power dependent on the Kirchhoff mean effective stress:

$$K = k\, p_a \left(\frac{\bar{p}_0}{p_a}\right)^n \frac{\bar{p}_0^2\,(1-n) + n\pi^2}{p_0^2} \tag{3a}$$

$$G = \frac{g}{1-n} p_a \left(\frac{\bar{p}_0}{p_a}\right)^n \frac{\bar{p}_0^2\; - n\pi^2}{\bar{p}_0^2} \tag{3b}$$

$$J = kn\; q\pi\; p_a^{1-n} \bar{p}_0^{n-2} \tag{3c}$$

where $\bar{p}_0$ is a measure of stress which is function of Kirchhoff mean effective stress π and Kirchhoff deviatoric invariant q.

$$\bar{p}_0^2 = \pi^2 + \frac{k(1-n)q^2}{3g} \tag{4}$$

2.2 *Yield surface*

The yield surface of the SIMSAND model is a cone with its apex in the origin, as presented in Figure 1. The yield is defined as the difference between the stress ratio $\eta = q/\pi$ and the yield stress ratio M_h.

$$f = \eta - M_h \tag{5}$$

The yield stress ratio M_h is defined by Equation (6), which results in non-linear behaviour during monotonic loading, where the stress ratio η approaches the available peak stress ratio M_p asymptotically.

$$M_h = M_p \frac{\epsilon_d^p}{k_p + \epsilon_d^p} \tag{6}$$

where k_p is a material parameter that controls the plastic stiffness, and ϵ_d^p is the deviatoric plastic strain defined as:

$$\epsilon_d^p = \sqrt{\frac{2}{3}\,\mathrm{dev}(\boldsymbol{l}^p):\mathrm{dev}(\boldsymbol{l}^p)} = \sqrt{\frac{2}{3}\,\mathrm{dev}\left(\dot{\gamma}\frac{\partial G}{\partial \boldsymbol{\tau}}\right):\mathrm{dev}\left(\dot{\gamma}\frac{\partial G}{\partial \boldsymbol{\tau}}\right)} \tag{7}$$

where dev stands for the deviatoric part of a tensor, $\boldsymbol{l}^p$ is the plastic velocity gradient, $\dot{\gamma}$ is the plastic multiplier and G is the plastic potential.

Equation (6) is a hyperbolic function of the deviatoric plastic strain ϵ_d^p. Consequently, this variable is the hardening variable in the model and controls the size of the yield surface.

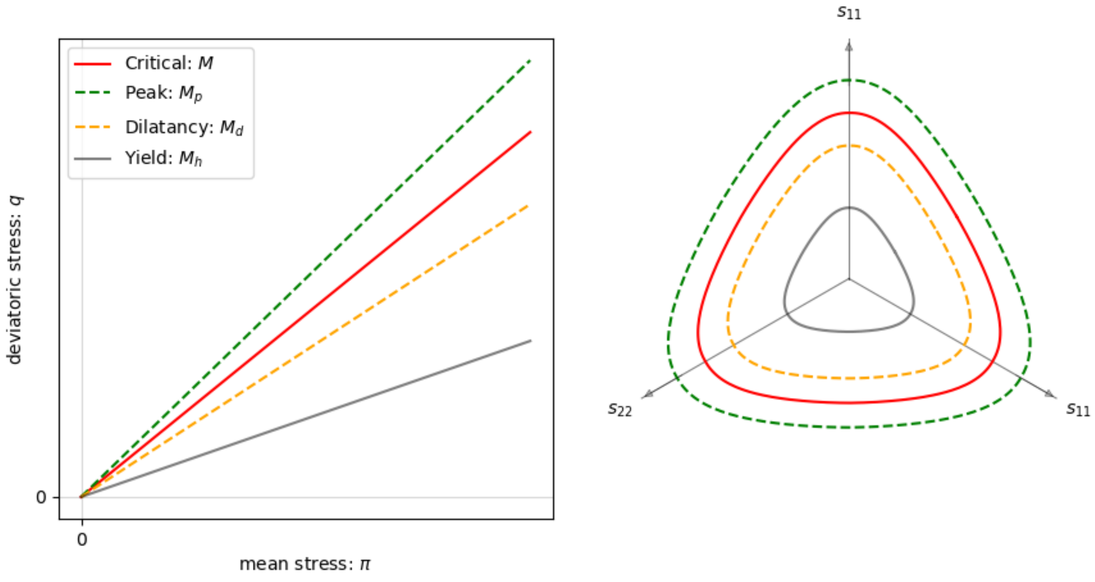

Figure 1 Yield surface of SIMSAND model

2.3 *Dilatancy*

The model is non-associated and uses a nonlinear stress-dilatancy relation based on the Nova-Wood rule (Nova & Wood, 1979). This is written as:

$$D = \frac{\delta l_{ii}^p}{\delta \epsilon_d^p} = A_d(M_d - \eta) \tag{8}$$

where A_d is a parameter controlling the magnitude of stress-dilatancy and M_d is the dilatancy stress ratio, depicted in Figure 1 as a dashed orange line. M_d is also known as the phase transformation stress ratio (Ishihara et al., 1975), because it defines a transitional state between contractile behaviour when $\eta < M_d$ and dilatant behaviour for $\eta > M_d$ and null dilatancy for $\eta = M_d$.

2.4 *Critical state*

The critical state of a soil, characterised by continuous shear deformation without volume change, is attained when the soil concurrently reaches both a critical stress ratio $q_c/\pi_c = M$ and a critical void ratio e_c within the compression space (Schofield & Wroth, 1968; Wood, 1991). In order to define this condition, a critical state line (CSL) is defined as a straight line in the space $\pi - q$ (red line in Figure 1), while the CSL in the compression plane (void ratio e - mean effective stress π) is defined as a non-linear relationship in a semilogarithmic plane following the exponential form proposed by Gudehus (1997):

$$e_{cs} = e_{c0} \exp\left(-\lambda_c \left(\frac{p'}{p_{atm}}\right)^{\xi}\right) \tag{9}$$

where e_{c0} is the critical void ratio for zero mean effective stress, λ_c controls the position of the inflection point and ξ controls the slope after the inflexion point.

The utilisation of this exponential form of the CSL in the compression plane aligns with the findings of various authors (Been & Jefferies, 1985; Pestana & Whittle, 1995). This non-linearity is believed to result from the crushing of grains under high stress (Coop & Lee, 1992; Wood, & Maeda, 2008). Equation (9) is preferred over other non-linear relations (Li and Wang, 1998) because its exponential form ensures there is no negative critical void ratio at high mean effective stress.

The model is made critical-state dependent by defining the peak stress ratio M_p, and the phase transformation stress ratio M_d, function of the state parameter $\psi = e - e_c$ (Been & Jefferies, 1985) This dependency follows the exponential equations defined by Li and Dafalias (2000):

$$M_p = M \exp(-n_p \psi) \tag{10a}$$

$$M_d = M \exp(n_d \psi) \tag{10b}$$

where n_p and n_d are material parameters that define the rate of evolution of M_p and M_d with the state parameter ψ. With the above definitions, there are three possible conditions: (i) For dense than critical condition ($\psi < 0$, presented in Figure 1), where $M_p > M > M_d$; (ii) For loose than critical condition ($\psi > 0$), where $M_d > M > M_p$; and (iii) for $\psi = 0$, where $M_p = M = M_d$. Then, during shear loading as $\psi \rightarrow 0$, M_p and M_d go to the critical stress ratio M, resembling a pair of closing scissors (Dafalias & Manzari, 2004).

2.5 Third invariant effect

The effect of the third invariant is considered defining the critical stress ratio M a function of the Lode angle θ. The equation defined by Sheng et al. (1999) is used to interpolate the critical stress ratio in triaxial compression M_c and extension M_e:

$$M(\theta) = M_c \left(\frac{2\alpha^4}{1 + \alpha^4 - (1 - \alpha^4)\sin 3\theta}\right)^{1/4} \tag{11}$$

where α is the ratio between the critical stress ratio in triaxial extension and compression, $\alpha = M_e/M_c$. The Lode angle is $\theta = +30º$ for triaxial compression and $\theta = -30º$ for triaxial extension.

The dependency of M on the Lode angle θ produces that M_p, M_d and M_h are also a function of Lode angle as depicted in Figure 1. The variation of $M(\theta)$ given by Equation (12) produces a smooth and continuously differentiable function in the deviatoric plane, which is also convex for $\alpha > 0.6$ (Sheng et al., 1999).

$$M(\theta) = M_c \left(\frac{2\alpha^4}{1 + \alpha^4 - (1 - \alpha^4)\sin 3\theta} \right)^{1/4} \tag{12}$$

3 Numerical implementation

The SIMSAND model in G-PFEM follows a finite-strain formulation, using a multiplicative decomposition of the deformation gradient into elastic and plastic part $F_{ij} = F^e_{ik} F^p_{kj}$ (Simo & Hughes, 1998). The constitutive model is locally integrated using an explicit integration scheme based on Monforte et al. (2015), which extends the modified Euler algorithm with adaptive sub-stepping developed by Sloan et al. (2001) to large strains, hyperelastic-plastic models. A summary of this algorithm is illustrated in Figure 2.

```
Input:
  Initial elastic left Cauchy Green tensor: $\boldsymbol{b}^e_n = \boldsymbol{F}^e_n \cdot \boldsymbol{F}^{eT}_n = \exp(2\boldsymbol{\epsilon}^e)$
  Initial hardening parameters: $\chi_n = \epsilon^p_{d_n}$
  Initial Kirchhoff stress tensor: $\boldsymbol{\tau}_n = \partial_{\boldsymbol{b}^e} W(\boldsymbol{b}^e_n)$
  Deformation gradient increment: $\mathbf{f}^{n+1}_n = \boldsymbol{F}_{n+1} \cdot \boldsymbol{F}^{-1}_n$
// compute elastic trial state
$\boldsymbol{b}^{e,trial} = \mathbf{f}^{n+1}_n \cdot \boldsymbol{b}^e_n \cdot \mathbf{f}^{n+1^T}_n$
$\boldsymbol{\tau}^{trial} = \partial_{\boldsymbol{b}^e} W(\boldsymbol{b}^{e,trial})$
if $f(\boldsymbol{\tau}^{trial}, \chi_n) < Tol$   // elastic step
|...  $\boldsymbol{b}^e_{n+1} = \boldsymbol{b}^{e,trial}, \chi_{n+1} = \chi_n$
else  // elasto-plastic step
|... if $f(\boldsymbol{\tau}_n, \chi_n) < -Tol$ or $\partial_{\boldsymbol{\tau}} f \cdot \boldsymbol{\tau}^{trial} < 0$  // Find yield surface intersection
|... |...Find $\alpha$ such that $f(\boldsymbol{\tau}_{n+\alpha}, \chi_n) = 0$, where $\boldsymbol{\tau}_{n+\alpha} = \partial W_{\boldsymbol{b}^e}(\boldsymbol{b}^e_{n+\alpha})$ and $\boldsymbol{b}^e_{n+\alpha} = \mathbf{f}^{n+\alpha}_n \cdot \boldsymbol{b}^e_n \cdot \mathbf{f}^{n+\alpha^T}_n$
|... else
|... |... $\alpha = 0$
|... end  // Integrate remaining increment $\boldsymbol{f}^{n+1}_{n+\alpha}$
|... adaptive sub-stepping with error control by Sloan et al. (2001): get $\boldsymbol{b}^e_{n-1}$ and $\chi_{n+1}$
|... consistent drift correction by Potts and Gens (1985): adjust $\boldsymbol{b}^e_{n\mp1}$ and $\chi_{n+1}$ keeping $\mathbf{f}^{n+1}_n$ unchanged
end
$\boldsymbol{\tau}_{n+1} = \partial_{\boldsymbol{b}^e} W(\boldsymbol{b}^e_{n+1})$
Output: $\boldsymbol{b}^e_{n+1}, \boldsymbol{\tau}_{n+1}, \chi_{n+1}$
```

Figure 2 Scheme of the explicit stress integration algorithm for large strain hyperelastic -plastic models according to Monforte et al. (2015)

In the above algorithm, the Kirchhoff stress tensor is computed from a free energy that is function of the elastic left Cauchy Green tensor $W^*(b^e_{ij})$. This free energy is related to the free energy function presented in Equation (1) by the following expression, as a result of the hyper-elastic formulation.

$$\boldsymbol{\tau} = 2\frac{\partial W^*(\boldsymbol{b}^e)}{\boldsymbol{b}^e} \cdot \boldsymbol{b}^e = \frac{\partial W(\boldsymbol{\epsilon}^e)}{\boldsymbol{\epsilon}^e} \tag{13}$$

For solving boundary value problems, the local integration of the constitutive model is hosted in the more computationally efficient IMPLEX technique proposed by Oliver et al. (2008), as well as a non-local formulation based on Galavi and Schweiger (2010). These methodologies improve global convergence, particularly in scenarios involving material softening, where the stiffness matrix can become ill-conditioned. Additionally, they contribute to reducing the mesh dependency of the solution. Details regarding the implementation of these two algorithms can be found in Monforte et al. (2019).

4 Validation

This section presents the results of numerically simulated triaxial tests using a single Gauss point (element tests) and boundary-value problems. All the simulations presented correspond to a material calibrated to replicate the behaviour of Fontainebleau sand NE34. The calibrated parameters of this material are provided in Table 1.

Table 1 SIMSAND parameters for Fontainebleau sand NE34

Parameter	**Value**
Shear stiffness factor: g	200.0
Poisson ratio: ν	0.15
Critical stress ratio: M	1.30
Extension compression ratio: α	0.70
Critical void ratio for $\pi = 0$: e_{c0}	0.76
Position CSL: λ_c	0.0044
Exponent CSL: ξ	0.90
Plastic modulus: k_p	0.0018
Peak factor: n_p	1.80
Multiplier dilatancy: A_d	0.55
Dilatancy factor n_d	2.20

4.1 Elementary test

The first simulation to validate the numerical implementation of SIMSAND in G-PFEM is an element test (one Gauss point) of a drained triaxial test. Figure 3 depicts the deviatoric stress – axial strain response and the evolution of void ratio in the compression plane. Three conditions are evaluated: first, a sample with an initial mean effective stress of $p_0 = 100$ kPa and initial void ratio of $e_0 = 0.81$, which corresponds to an initial loose than critical sample. Second, a sample initially dense than critical with $p_0 = 100$ kPa and $e_0 = 0.66$, and finally, a sample with $p_0 = 400$ kPa and $e_0 = 0.636$, which also corresponds to an initial dense than critical sample.

The numerical simulations are compared with the experimental tests carried out by Seif El Dine et al. (2010). As shown in Figure 3 the numerical simulations align with the experimental results, capturing the contraction of the loose sample, as well as the changes in contraction and dilation, along with the peak and softening behaviour of the initial dense than critical sample. It is worth noting that the simulation of the drained triaxial tests involves a mixed stress-strain condition requiring a non-linear iterative solver. Therefore, these results validate not only the local integration of the SIMSAND model but also the tangent elastoplastic matrix used for the Newton-Raphson iterations in the global integration.

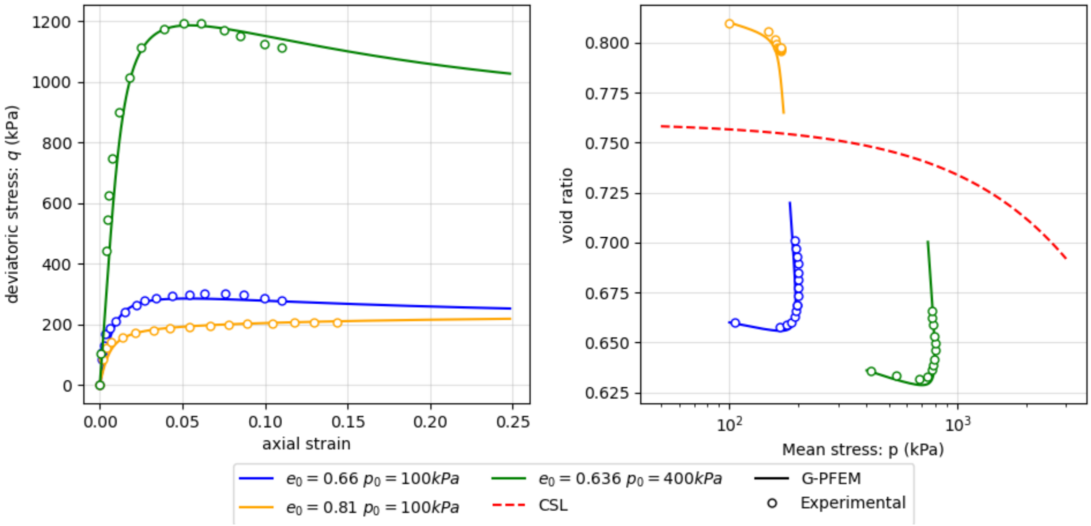

Figure 3 Elementary test simulation of drained triaxial test in Fontainebleau sand NE34.

The numerical simulation of two undrained triaxial test is reported in Figure 4. The first test corresponds to an initial dense than critical material with $e_0 = 0.72$ and $p_0 = 100$ kPa. For this condition the material experiences first a reduction in the mean effective stress as a consequence of a contraction tendency, but after the stress ratio reaches M_d, there is a phase transformation and the mean effective stress increases. At the end of the simulation, this sample does not reach the critical state, so there is still an increase in the deviatoric stress. The second test corresponds to an initial loose than critical soil with the same p_0 but and initial void ratio of 0.78. In this case, the material experiences a reduction in the mean effective stress until it reaches a liquefaction state ($p \rightarrow 0$).

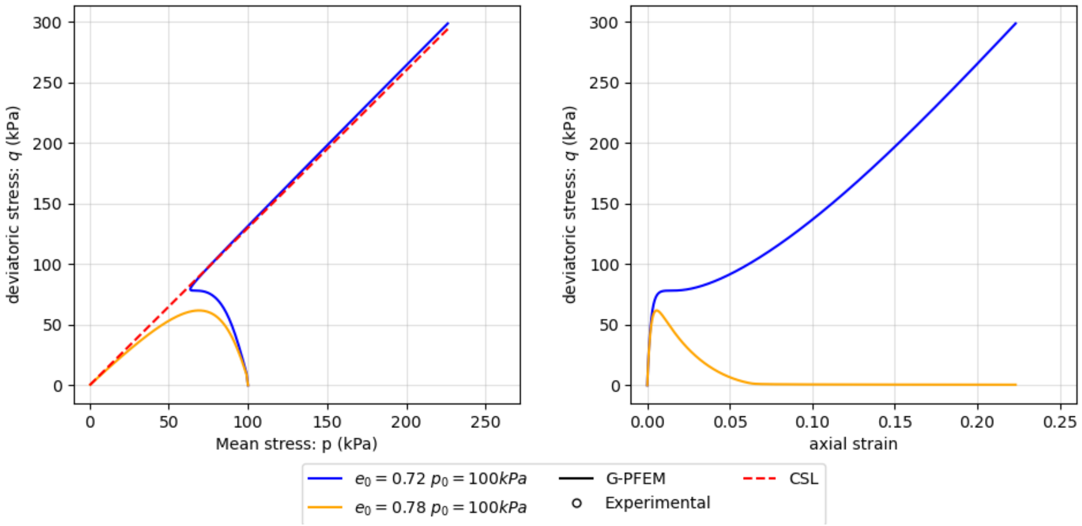

Figure 4 Elementary test simulation of undrained triaxial test in Fontainebleau sand NE34.

4.2 Boundary value problem

Using a boundary value problem, a series of drained triaxial tests were conducted to validate the implementation of SIMSAND in G-PFEM for a large deformation problem. This process contemplated a remeshing process to address the large deformation problem, as well as the use of the IMPLEX integration and the non-local formulation. A two-dimensional axisymmetric model with dimensions of 0.1 m in height and 0.05 m in width was used, in which a vertical displacement of 0.05 m was applied on the top boundary. The initial state of the soil was deemed isotropic with $p_0 = 200$ kPa.

Two conditions were evaluated. First, a smooth contact condition between the upper plate of the triaxial cell and the soil was considered, so that the top boundary could move freely in the horizontal direction. Second, a rough contact condition, in which the horizontal displacements of the top boundary were restricted. The former condition results in a homogeneous deformation process, whereas the latter causes a non-homogeneous deformation with strain localization. In both cases, three different initial void ratios were analysed, covering initial loose and dense than critical materials.

Figure 5 depicted the results for the smooth contact conditions in terms of the stress-strain curve. The results are consistent with expectations, as the three samples predict the same critical strength but different peak strengths. The initial dense-than-critical state sample ($e_0 = 0.65$) predicts the highest peak value and significant post-peak strain softening. Figure 5b and c show the initial and final mesh for the sample with $e_0 = 0.75$. The initial number of elements is 184, and the final is 1196. As illustrated in the figure, the mesh maintains a favourable aspect ratio at the conclusion of the test, despite the sample reaching a high strain condition, which is a result of the G-PFEM remeshing process.

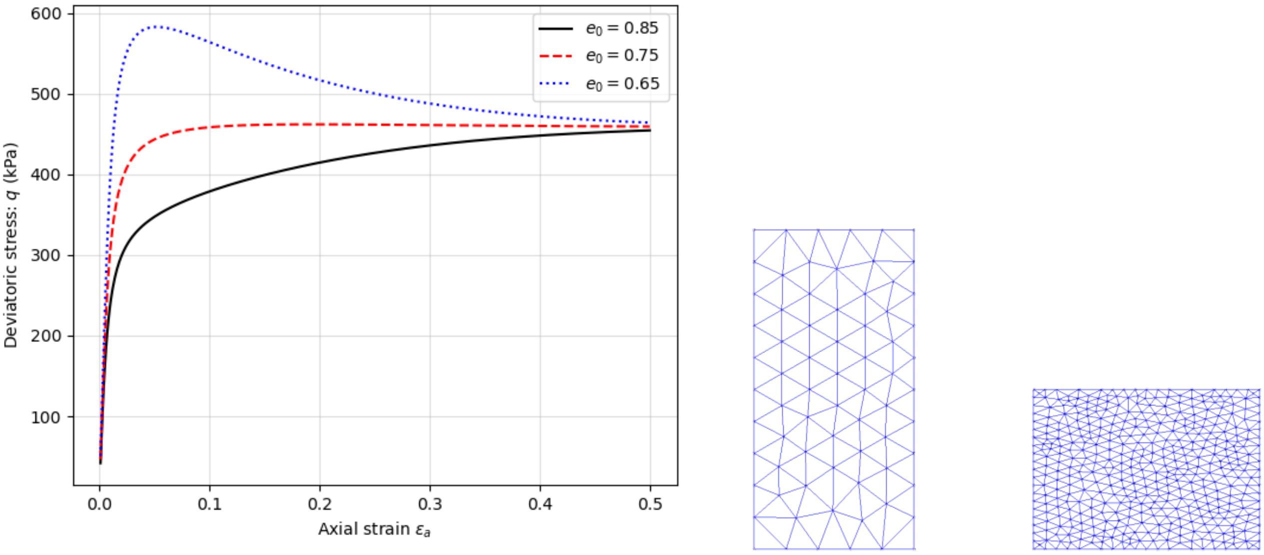

a) Stress strain response b) Initial mesh c) Final mesh

Figure 5 Boundary value simulation of drained triaxial test in Fontainebleau sand NE34 – smooth contact.

The results for the rough contact conditions are presented in Figure 6. Before the peak strength, the stress-strain curve is similar to that of the smooth contact condition. However, deformation is localized in a shear band that extends from the upper right to the lower left corner after the peak strength. This region is where smaller mesh elements are produced as a result of the remeshing criterion in G-PFEM, based on plastic straining. The initial and final mesh for the sample with $e_0 = 0.75$ is shown in Figure 6; the initial number of elements is 184, while the final is 970.

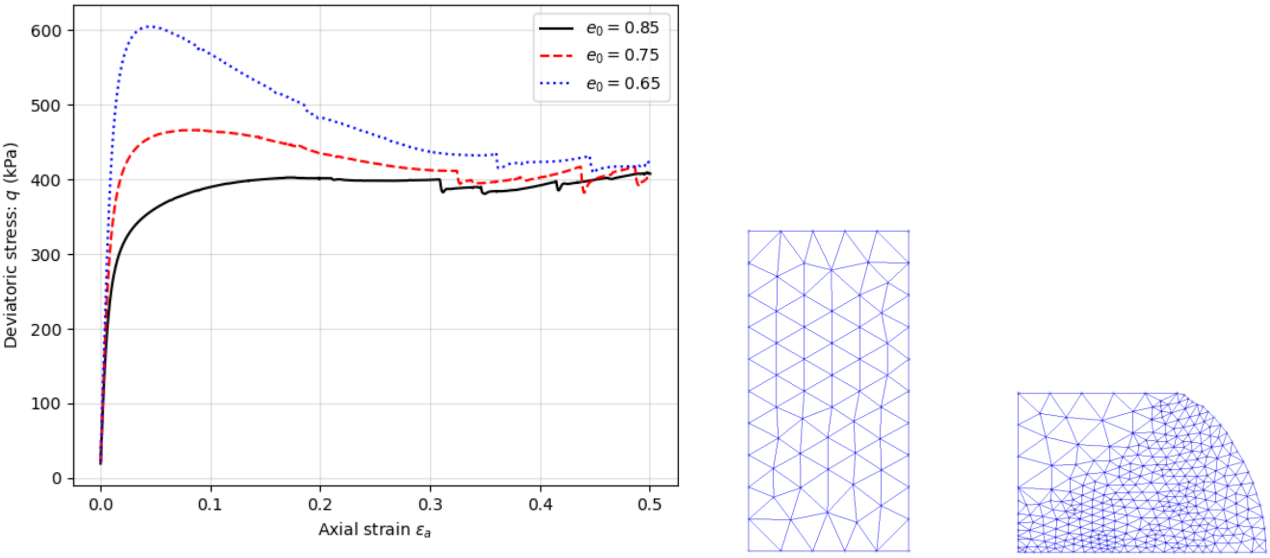

a) Stress strain response b) Initial mesh c) Final mesh

Figure 6 Boundary value simulation of drained triaxial test in Fontainebleau sand NE34 – rough contact.

5 Conclusion

The implementation of the SIMSAND model in G-PFEM was presented. The model accounts for the dependency of the state parameter in the peak strength and volumetric response, which allows capturing the typical behaviour of drained dense sand, such as the transformation phase between contraction and dilation, as well as softening after the peak strength or softening in undrained loose sands. The formulation of SIMSAND is adapted to finite strain theory using a multiplicative decomposition of the deformation gradient and a hyper-elastic model. The accuracy of the implementation was confirmed through element testing and boundary value problems, employing an IMPLEX integration scheme and a non-local formulation. In future applications, this constitutive model will be used for the simulation of cone penetration tests (CPT) and pile installation in sandy soils.

Credit authorship contribution statement

D. León-Vanegas: Conceptualization, Methodology, Software, Writing – original draft. **L. Monforte.**: Conceptualization, Methodology, Writing – review & editing. **M. Arroyo**: Conceptualization, Funding acquisition, Writing – review & editing.

Declaration of competing interests

The authors declared that there is no conflict of interests.

Acknowledgments

The authors gratefully acknowledge financial support provided by the European Union ’s Horizon Europe Programme under the Marie Skłodowska–Curie actions HORIZON-MSCA-2021-DN-01 call (Grant agreement ID: 101072360).

6 References

Been, K., & Jefferies, M. G. (1985). A state parameter for sands. *Géotechnique*, *35*(2), 99–112. https://doi.org/10.1680/geot.1985.35.2.99

Carbonell, J. M., Monforte, L., Ciantia, M. O., Arroyo, M., & Gens, A. (2022). Geotechnical particle finite element method for modeling of soil-structure interaction under large deformation conditions. *Journal of Rock Mechanics and Geotechnical Engineering*, *14*(3), 967–983. https://doi.org/10.1016/j.jrmge.2021.12.006

Coop, M. R., & Lee, I. K. (1992). The behaviour of granular soils at elevated stresses. In G. T. Houlsby & A. N. Schofield (Eds.), *Predictive soil mechanics: Proceedings of the Wroth Memorial Symposium held at St Catherine's College, Oxford, 27-29 July 1992* (p. 0). Emerald Publishing Limited. https://doi.org/10.1680/psm.19164.0012

Dafalias, Y. F., & Manzari, M. T. (2004). Simple Plasticity Sand Model Accounting for Fabric Change Effects. *Journal of Engineering Mechanics*, *130*(6), 622–634. https://doi.org/10.1061/(ASCE)0733-9399(2004)130:6(622)

Dine, B. S. E. (2010). *Etude du comportement mécanique de sols grossiers à matrice*.

Gajo, A., & Wood, M. (1999). Severn–Trent sand: A kinematic-hardening constitutive model: the *q–p* formulation. *Géotechnique*, *49*(5), 595–614. https://doi.org/10.1680/geot.1999.49.5.595

Galavi, V., & Schweiger, H. F. (2010). Nonlocal Multilaminate Model for Strain Softening Analysis. *International Journal of Geomechanics*, *10*(1), 30–44. https://doi.org/10.1061/(ASCE)1532-3641(2010)10:1(30)

Houlsby, G. T., Amorosi, A., & Rojas, E. (2005). Elastic moduli of soils dependent on pressure: A hyperelastic formulation. *Géotechnique*, *55*(5).

Hu, W., Yin, Z., Dano, C., & Hicher, P.-Y. (2011). A constitutive model for granular materials considering grain breakage. *Science China Technological Sciences*, *54*(8), 2188–2196. https://doi.org/10.1007/s11431-011-4491-0

Ishihara, K., Tatsuoka, F., & Yasuda, S. (1975). Undrained Deformation and Liquefaction of Sand Under Cyclic Stresses. *Soils and Foundations*, *15*(1), 29–44. https://doi.org/10.3208/sandf1972.15.29

Jefferies, M. G. (1993). Nor-Sand: A simle critical state model for sand. *Géotechnique*, *43*(1), 91–103. https://doi.org/10.1680/geot.1993.43.1.91

Leon-Vanegas, D., Monforte, L., Arroyo, M., & Gens, A. (2025). A constitutive model accounting for grain crushing in silica sands. *ISSMGE*. 5th International Symposium on Frontiers in Offshore Geotechnics ISFOG. https://doi.org/10.53243/ISFOG2025-136

Li, X. S., & Dafalias, Y. F. (2000). Dilatancy for cohesionless soils. *Géotechnique*, *50*(4), 449–460. https://doi.org/10.1680/geot.2000.50.4.449

Monforte, L., Arroyo, M., Gens, A., & Carbonell, J. M. (2015). Explicit finite deformation stress integration of the elasto-plastic constitutive equations. *Proceedings of the XII International Conference on Computational Plasticity – Fundamentals and Application*. Computational Plasticity XIII – Fundamentals and Applications.

Monforte, L., Ciantia, M. O., Carbonell, J. M., Arroyo, M., & Gens, A. (2019). A stable mesh-independent approach for numerical modelling of structured soils at large strains. *Computers and Geotechnics*, *116*, 103215. https://doi.org/10.1016/j.compgeo.2019.103215

Nova, R., & Wood, D. M. (1979). A constitutive model for sand in triaxial compression. *International Journal for Numerical and Analytical Methods in Geomechanics*, *3*(3), 255–278. https://doi.org/10.1002/nag.1610030305

Oliver, J., Huespe, A. E., & Cante, J. C. (2008). An implicit/explicit integration scheme to increase computability of non-linear material and contact/friction problems. *Computer Methods in Applied Mechanics and Engineering*, *197*(21–24), 1865–1889. https://doi.org/10.1016/j.cma.2007.11.027

Pestana, J. M., & Whittle, A. J. (1995). *Compression model for cohesionless soils*.

Rowe, P. W. (1962). The stress-dilatancy relation for static equilibrium of an assembly of particles in contact. *Proceedings of the Royal Society of London. Series A. Mathematical and Physical Sciences*, *269*(1339), 500–527. https://doi.org/10.1098/rspa.1962.0193

Schofield, A., & Wroth, P. (1968). *Critical State Soil Mechanics*.

Sheng, D., Sloan, S., & Yu, H. (1999). Practical Implementation of Critical State Models in FEM. *Australia-New Zealand Conference on Geomechanics (8th: 1999: Hobart, Tas.)*, 975–981.

Simo, J. C., & Hughes, T. J. R. (1998). *Computational Inelasticity* (Vol. 7). Springer-Verlag. https://doi.org/10.1007/b98904

Sloan, S. W., Abbo, A. J., & Sheng, D. (2001). Refined explicit integration of elastoplastic models with automatic error control. *Engineering Computations*, *18*(1–2), 121–194. https://doi.org/10.1108/02644400110365842

Taiebat, M., & Dafalias, Y. F. (2008). SANISAND: Simple anisotropic sand plasticity model. *International Journal for Numerical and Analytical Methods in Geomechanics*, *32*(8), 915–948. https://doi.org/10.1002/nag.651

Wood, D. M. (1991). *Soil Behaviour and Critical State Soil Mechanics* (1st ed.). Cambridge University Press. https://doi.org/10.1017/CBO9781139878272

Wood, D. M., & Maeda, K. (2008). Changing grading of soil: Effect on critical states. *Acta Geotechnica*, *3*(1), 3–14. https://doi.org/10.1007/s11440-007-0041-0

Yin, Z.-Y., Hicher, P.-Y., & Jin, Y.-F. (2020). Elastoplastic Modeling of Soils: From Mohr-Coulomb to SIMSAND. In Z.-Y. Yin, P.-Y. Hicher, & Y.-F. Jin, *Practice of Constitutive Modelling for Saturated Soils* (pp. 121–176). Springer Singapore. https://doi.org/10.1007/978-981-15-6307-2_5